ARTICLE OPEN

Check for updates

Leaf-meridian bio-inspired nanofibrous electronics with uniform distributed microgrid and 3D multi-level structure for wearable applications

Mingxu Wang[1,2], Li Dong[1,2], Jiajia Wu[1,2], Jian Shi[3], Qiang Gao[4], Chunhong Zhu[1,2,5]✉ and Hideaki Morikawa[1,2,5]✉

The interface between the active electronic and its osculatory target dominates the sensing response of high-sensitivity sensors. However, the interface properties are difficult to be adjusted and preserved owing to the limited strategies for surface engineering. In this work, inspired by nature frond leaf, a spatial multi-level nanofibrous membrane with grid-like microstructure of uniform distribution was fabricated, in which carboxylated carbon nanotubes (CCNTs)/poly(3,4-ethylenedioxythiophene) (PEDOT) was modified onto the surface of grid-like polyurethane (PU) nanofiber *via* the combination of metal mesh template, in situ polymerization and ultrasonic treatment. Nanofibrous membrane enables a pressure sensor with high sensitivities (5.13 kPa^{-1}), fast response/recovery time (80 ms and 120 ms), and ultralow detection limit of 1 Pa. In addition, as a scalable and integrable platform, we also demonstrate its multifunctional applications for electro-thermal conversion and energy harvesting. All these results indicate the proposed nanofibrous membrane may potentially be applied to next-generation wearable devices.

npj Flexible Electronics (2022)6:34 ; https://doi.org/10.1038/s41528-022-00171-x

INTRODUCTION

Flexible electronic device is one of the key components in the next-generation health monitoring, human-machine interface, soft robotics and so forth[1–4]. Especially, wearable sensors (pressure and strain sensors, humidity sensors, temperature sensors, and so on) have gained considerable attention as they can transduce the physical stimulation (human behaviors or environments) into electronic signals[5–7]. So far, significant advancements have been achieved in previous works to fabricate these sensors with high performance, comfortable attachment, long service life, and technological compatibility[5,8,9]. Typical examples include varieties of gel[10,11], composite polydimethylsiloxane-based (PDMS) conductive elastomers[12,13], and other modified conductive Ecoflex[14–16]. Despite the superior flexibility and electroactivity, it seems to be difficult for us to associate them with comfortability, especially the poor but vital breathability, moisture penetrability and lightness, and even skin-friendly characters. Also, a single feature capability is far from sufficient to meet usage expectations for increasingly complex systems, integration of multifunctional properties for practical application of electronic devices is highly desirable. Therefore, the trade-off between these mentioned and expanding functionality or sufficient comfortability remains a huge challenge.

Recently, electrospinning nanofibers seem to provide us with an attractive platform owing to their promising advantages and properties in flexibility, high surface area, and diverse fibrous morphologies[17–19]. As a successful commercial representative, large-scale and repeatable production of nanofibers with adjustable diameters (from nanometers to micrometers) has been realized[20]. Viable nanofiber assemblies present compelling allure and dominance in the design and fabrication of thin, soft, lightweight, breathable, and comfortable electronic devices. Especially, introduce of biocompatible matrix enables it ideal to applied directly interface with tissues, organs or cells[21,22], which further broadens the potential applicability in the biomedical field. Therefore, nanofiber-based sensors have been widely investigated as building blocks for flexible electronic devices.

Moreover, practically, one of the critical parameters affecting the performance of sensors is the ability to operate in a wide range with high sensitivity and stable linear ranges[23,24]. For this issue to be addressed, the novel structural design, such as pyramids[25], cylinders[26], hemispheres[27], and hierarchical structure[28], becomes an increasingly popular strategy inspired by the human skin and some of interesting interface morphologies widely existed in nature. Microstructures are advantageous for rational design of the sensors due to their well-defined structures, of which the high compressibility enables it to deform even under low external stimulation and reduces the negative influence from viscoelasticity and hysteresis effect of the substrate polymer and thus increases the response rate[29]. For instance, Wang et al.[30] designed an ultrasensitive all-textile airflow sensor based on carbonized silk fabric (CSF) with in situ grown of fluff-like carbon nanotubes (CNTs) as enhanced contact point. Yu et al.[31] prepared spinosum microstructure pressure sensors *via* an abrasive paper template for higher sensitivity and wider detection range. Zhu et al.[32] provided an enhancing idea based on folding structure and verified its validity through theoretical modeling analysis and comparison of three kinds of commonly used sensors practically (resistive, capacitive, and inductive sensor). Despite multiple works and efforts that have been obtained as above-mentioned, interesting strategies of structural design for improving the sensing performance of nanofibrous membrane-based pressure sensors is still very scarce. Most reports have focused on surface modification of single nanofiber, including the introduction of varieties of nanowires, nanosheets, and nanoparticles that optimizing surface roughness. However, it usually suffers from

[1]Graduate School of Medicine, Science and Technology, Shinshu University, 3-15-1 Tokida, Ueda, Nagano, Japan. [2]Institute for Fiber Engineering (IFES), Interdisciplinary Cluster for Cutting Edge Research (ICCER), Shinshu University, 3-15-1 Tokida, Ueda, Nagano, Japan. [3]Faculty of Systems Science and Technology, Akita Prefectural University, 84-4 Aza Ebinokuchi, Tsuchiya, Yurihonjo, Akita, Japan. [4]School of Chemistry and Chemical Engineering, Yangzhou University, Yangzhou, China. [5]Faculty of Textile Science and Technology, Shinshu University, 3-15-1 Tokida, Ueda, Nagano, Japan. ✉email: zhu@shinshu-u.ac.jp; morikaw@shinshu-u.ac.jp

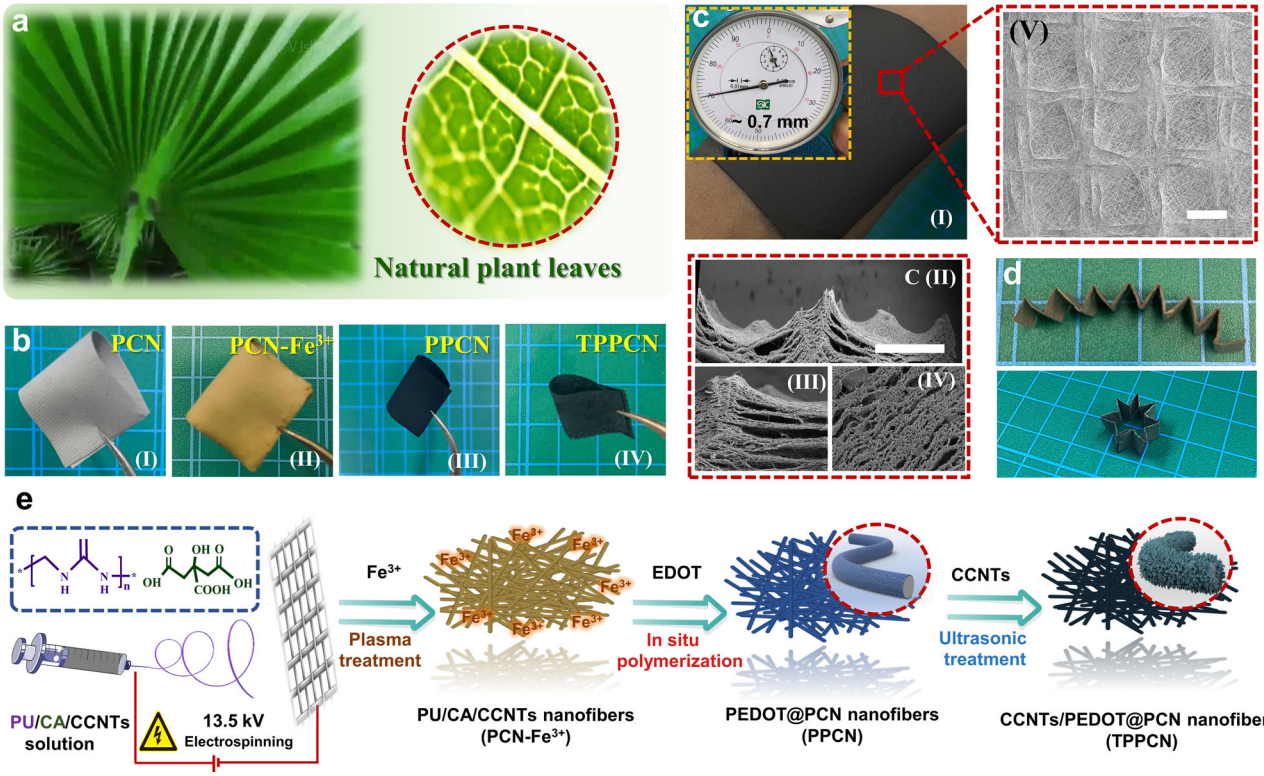

Fig. 1 Technological route of preparation mimicking meridian system of nature frond leaves. a Photograph of nature plant leaves with special meridians. **b** Digital images of different prepared nanofibrous membrane. **c** TTPCN membrane with thickness of 0.7 mm shows special grid-like morphology and multi-level structure, both the scale bars in **c (II)** and **c (V)** are 500 μm. **d** TTPCN membrane shows good flexibility. **e** Typical fabrication process of TPPCN membrane.

limitations of poor substrate selectivity, high cost, high technical difficulty, unstable processing quality, low service life and so on. A universal, simple and cost-effective strategy to improve the performance of nanofiber membrane-based sensing performance is still urgently needed.

With the above aim, herein, we propose a strategy for preparing a multifunctional nanofibrous membrane. Carboxylated carbon nanotubes (CCNTs) doped polyurethane (PU) nanofiber is used as matrix, of which especially spatial multi-level structure and grid-like morphology are obtained by using a metal mesh template. Subsequently, the conductive composite of poly(3,4-ethylenedioxythiophene) (PEDOT) and CCNTs respectively are loaded onto the surface of the substrate to form enhanced dual conductive layers *via* the coupling technologies of in situ polymerization and ultrasonic treatment. Consequently, nanofiber membranes can be processed into wearable electronic textile such as pressure sensor, thermal heater, temperature sensor and nanogenerator with facile encapsulation and weaving. Moreover, theoretical simulation results of the multi-level structure and grid-like morphology were provided to shed light on the mechanism and high performance. Totally, this work combines multi-functions to ensure an intelligent and integrated e-textile in order to detect various physiological or environmental signals, thereby which potentially could promote more practical and environmentally friendly applications in human-machine interfaces and artificial intelligence.

RESULTS

Special morphology and structure of prepared TPPCN membrane

Figure 1 depicts the typical technological route of preparation mimicking meridian system of nature frond leaves (Fig. 1a) to obtain enhanced performance. The flexible substrate, an electrospinning PU/CCNTs (named PCN) membrane (Fig. 1b (I)) is firstly prepared using a metal mesh as receiving device. Fig. S1 is a digital picture of prepared PU membrane, showing an interesting grid-like morphology. Test results of the contact angle verify the transformation of properties from super-hydrophobicity to hydrophilicity (Fig. 2k) after plasma treatment. Subsequently, it can be observed the gray PCN turns yellow (Fig. 1b (II)) after immersion of EtOH-Fe^{3+} solution. Combined with the scanning results of EDS mapping and XRD, a uniform distribution of Fe and Cl elements (Fig. S2), indicating a healthy attachment of Fe^{3+}. Thereby, facile in situ polymerization of EDOT reacts on the surface of PCN-Fe^{3+}, followed by the ultrasonic treatment. Black conductive CCNTs/PEDOT@PCN (named TPPCN) membrane is finally obtained (Fig. 1b (IV)). Typical TPPCN membrane with thickness of 0.7 mm is shown in Fig. 1c. Grid-like morphology is perfectly preserved from substrate, as well as the multi-level structure revealed by the SEM images of cross-section (Fig. 1c (II–V)). Moreover, Fig. S3 shows a typical three-dimensional (3D) image of microgrid morphology. The regular grid-like structure is evenly distributed on the surface with a center height of around 50 μm. More importantly, TPPCN membrane also remains flexible enough to be bent and folded into some other shape (Fig. 1d).

More efforts are spared to investigate the variation of morphology and structure composition during the membrane forming. Compared with pure PU membrane, doping of CCNTs and CA significantly increase the conductivity of spinning solution, resulting in thinner and finer PCN nanofibers (Fig. 2a, b)[33]. The average diameter is reduced from approximately 0.76 to 0.53 μm. Treatment of EtOH-Fe^{3+} solution causes appreciable crimping and swelling (Fig. 2c), accompanied by little increase in diameter (0.64 μm). Afterward, it continues to increase to 0.77 μm after in situ polymerization of PEDOT for 18 h (Fig. 2d). PEDOT layer forms as irregular scales wrapped around the nanofibers, which is confirmed in Fig. S4 and results in a rough surface. Whereas, the

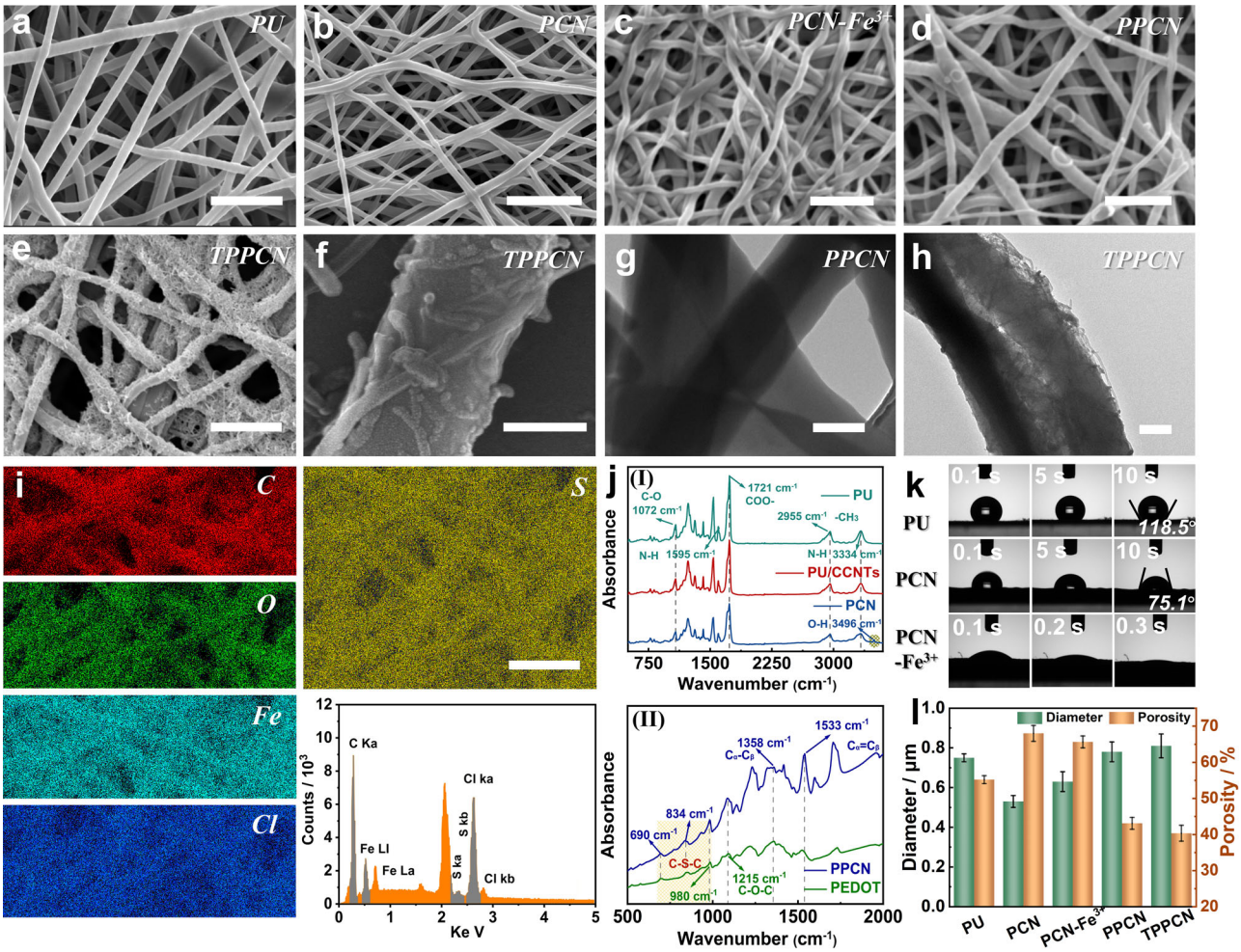

Fig. 2 Morphology and structure of prepared nanofibrous membranes. a–f SEM images of pure PU, PCN, PCN-Fe^{3+}, PPCN, and TPPCN membrane, the scale bars in **a**–**e** and **f** are 5 μm and 500 nm. **g**, **h** TEM images of PPCN and TPPCN membrane with core-shell structure and special morphology, both the scale bars in **g** and **h** are 500 nm. **i** EDS mapping results of TPPCN membrane, the scale bars in i is 5 μm. **j**–**l** FT-IR spectrums, contact angle, diameter, and porosity of prepared membranes. The error bars presented in the plots represent the standard deviations of the respective measurements.

3D porous networks structure is retained very well. Details of normal distribution for each sample's diameter are supplied in Fig. S5. Meanwhile, Fig. 2g demonstrates a TEM image of PPCN nanofibers, obvious core-shell structure with a continuous-coating PEDOT shell layer is observed. Furthermore, the CCNTs are anchored onto the surface of PCCN under the assistance of ultrasonication to prepare the TPPCN membrane. Naturally, more CCNTs would be anchored onto the PPCN nanofiber surface with prolonging ultrasonication time (Fig. S6). Time of 45 min is necessary, as shown in Fig. 2e. Many entangled CCNTs are observed to wrap on the nanofiber surface. Figure 2f, h are enlarged morphology of TPPCN membrane and TEM image. The porosity test results of the nanofiber membrane are shown in Fig. 2l. Totally the variation of porosity and diameter tends to be opposite, means that the larger the fiber diameter, the lower the porosity. And the polymerization significantly reduces the porosity. Finally, EDS mapping and XPS tests of the TPPCN membrane in Fig. 2i and S7 further demonstrates the uniform distribution of S (unique to PEDOT, Fig. S8 shows a typical chemical structure of PEDOT and anion polymerization process), Fe^{3+}, Cl, C and O elements on fiber surface.

Apart from the morphology and microstructure, FT-IR results (Fig. 2j) also confirm the composition variation of the fiber membrane during the preparation process. The characteristic bands at 1072 cm^{-1}, 1595 cm^{-1}, and 1721 cm^{-1} correspond to the stretching vibration of C-O, plane bending vibration of N-H and the free hydrogen-bonded carbonyl groups in the urethane linkage (-H-N-COO-) in the spectrum of pure PU, respectively. Also, peaks at 2955 cm^{-1} and 3334 cm^{-1} are caused by the stretching vibration of $-CH_3$ and overlap stretching vibration of N-H. Particularly, typical characteristic bonds belong to vibration of -OH is observed at 3496 cm^{-1} in the curve of PCN after the introduction of CA. For PPCN membrane, pure PEDOT sample prepared with the same process is tested to do a comparison. Accordingly, characteristic bands of PEDOT are observed, including the peaks at 1533 cm^{-1} and 1358 cm^{-1} of the carbon skeleton of thiophene ring, 690 cm^{-1}, 834 cm^{-1}, and 980 cm^{-1} attributed to the vibration of C–S–C and 1215 cm^{-1} belonged to C–O–C, respectively.

Electromechanical properties of TPPCN membrane

Prepared nanofibrous membrane exhibits good flexibility and stretchability. Typical tensile strain-stress curves of all samples are provided in Fig. 3a. Compared with pure PU membrane, doping of CCNT significantly improves the rigidity of PCN, which is consistence with previous works[23]. Also, sacrifice of mechanical performance is inevitable owing to repeated and long treatment, in

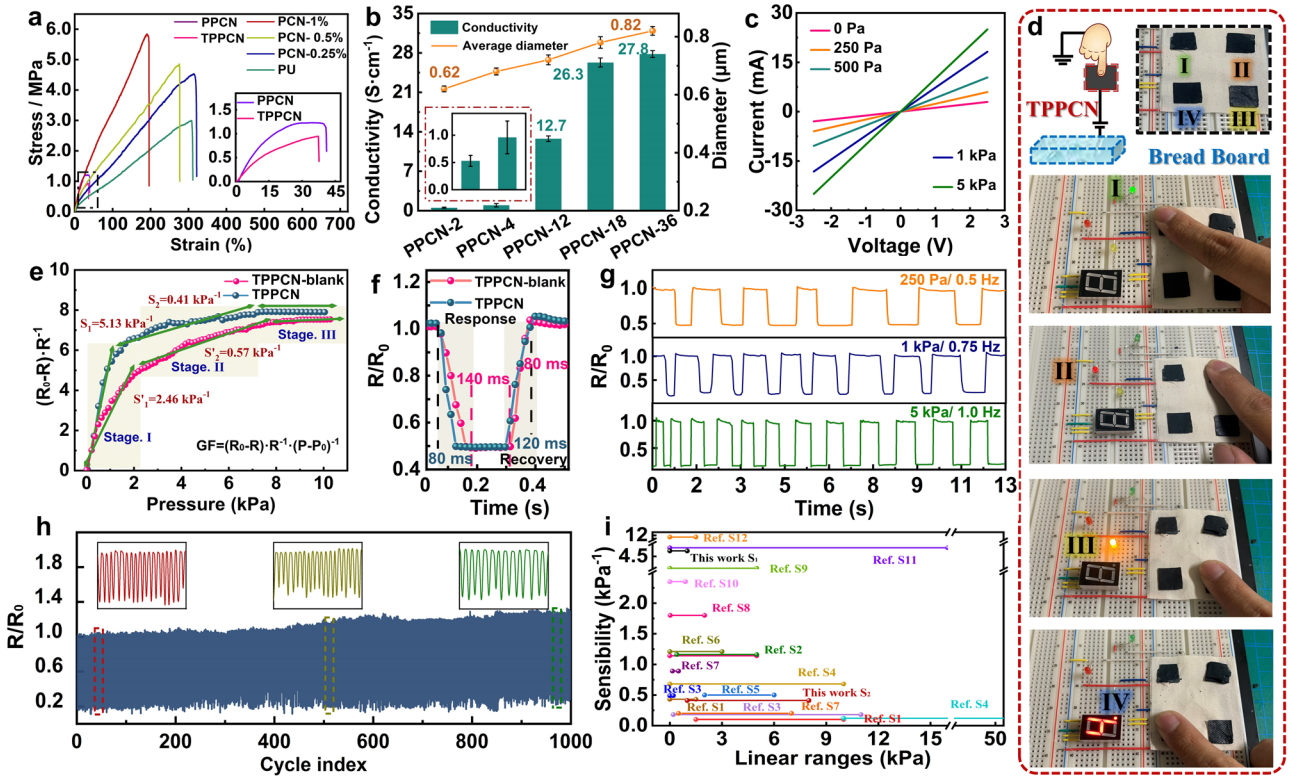

Fig. 3 Electromechanical properties of prepared nanofibrous membranes. a Typical tensile stress-strain curves of the prepared nanofibrous membrane. **b** Conductivity of PPCN membranes after in situ polymerization for different time. **c** *I–V* curves of the TPPCN membranes under different pressures. **d** Digital images of the touch sensors showing controlled lighting of LEDs through touching on the TPPCN membranes. **e**, **f** Comparison of the relative resistance change and response/recovery time of obtained TPPCN membrane with metal mesh template (TPPCN) and without special structure and morphology (TPPCN-blank) under an increased pressure. **g** Response of the TPPCN membrane with different pressure (0.25, 1.0 and 5.0 kPa) for various frequencies (0.5, 0.75, and 1.0 Hz). **h** 1000 loading/unloading process cycles toward the pressure variation from 0 to 500 Pa. **i** GF value of the TPPCN membrane compared with those reported in relevant literatures. The error bars presented in the plots represent the standard deviations of the respective measurements.

which substrate was wetted and dried by the solvent. PPCN membrane shows a reduced flexibility (1.21 MPa and 41.5%). Synchronously, the high energy of ultrasonic process will damage the nanofibrous structure. Thus, strength of TPPCN possess slight decrease (0.92 MPa), while there is no significant variation in elongation. Figure 3b shows the electrical conductivity of prepared samples with different situ polymerization time (2–36 h). Pure PU is no-conductive. Despite CCNT with content of 1 wt% is doped, resistance of PCN membrane cannot be tested by multimeter (å 10^9 Ω). While, conductivity of PPCN dramatically improves to ~0.5 S cm^{-1} only after in situ polymerization for 2 h. And it continues to increase to ~26.3 S cm^{-1} (18 h) with the prolonging polymerization time and increased fiber diameter. Especially, great stability and durability are confirmed by stable conductivity (Fig. S9), where PPCN membrane was placed in acid (pH = 2), alkali (pH = 12) and salt ion solution (NaCl, 0.1 M), ethanol for more than 6 h. However, as we mentioned long-term solvent immersion will seriously damage the structure of PPCN membrane, resulting in a sharp decline in mechanical properties. Even, the PPCN membrane becomes fragile and could not withstand further ultrasonic modification when the polymerization time exceeded 36 h. Time of 18 h is optimized and used as an appropriate final parameter in this work, after which conductivity will not increase obviously indicating a completely coating and conductive paths. Additionally, the existence of PEDOT layer has made the conductivity of the PPCN membrane at a high level and the modification by CCNTs would not further improve the conductivity of the TPPCN samples (Fig. S10 shows the conductivity of TPPCN membrane after ultrasonic treatment for different time). Due to the high conductivity, TPPCN membrane can be used as a conductor in the circuit to light a LED bulb or others electronic devices. We also show its application as touch sensors. In an interesting illustration, TPPCN membrane used as sensing units is weaved onto a cotton fabric with a formation of 2 × 2 integrated array enables an touch sensor (Fig. 3d). Another functional processor is manufactured in bread board, thus it could distinguish different touch positions as demonstrated by lighting the corresponding LEDs connected in the TPPCN membrane.

Furthermore, pressure sensing property is investigated using the TPPCN membrane as the target. The current-voltage (*I–V*) curves shown in Fig. 3c, depict the relative change of current varies with different applied pressure. The TPPCN membrane demonstrates linear *I–V* characteristics with a relatively stable response to pressure, and it is confirmed to the Ohm's law during the whole testing range. For the pressure sensitivity, gauge factor (GF) is used to evaluate the pressure sensitivity (*S*), and it is defined as

$$GF = \frac{R_0 - R}{R \times \Delta P} \quad (1)$$

where *R*, R_0 and *ΔP* denote the real-time, initial resistance, and variation in pressure, respectively. As shown in Fig. 3e, there are three linear resistance segments clearly can be found during the dynamic instantaneous resistance response to varying pressure, which detailly manifested as a sharp increase in the low-pressure range, a gradual increase in the intermediate-pressure and stable tendency in high-pressure range. Thus, it is correspondingly calculated to be of 5.13 (0–1.0 kPa) and 0.41 kPa^{-1} (1.0–8.0 kPa), respectively. Particularly, TPPCN membrane shows ultralow response limit. Although noise signals are unavoidable, it is

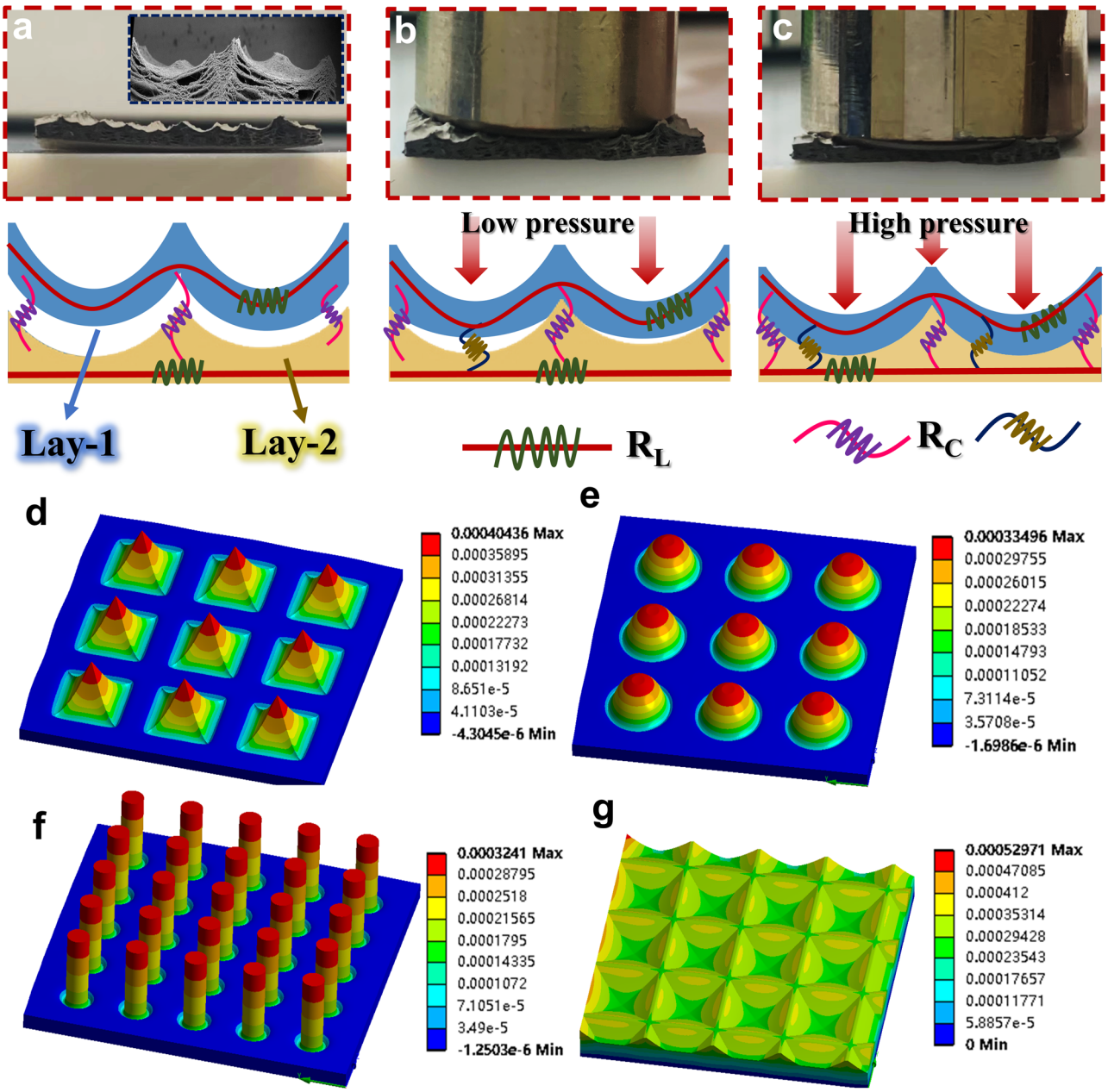

Fig. 4 Working mechanism and pressure simulation of TPPCN pressure sensor. a–c Photographs and schematic illustrations of equivalent circuit models corresponding to initial, low-pressure, and high-pressure states. **d–g** The simulation results of pressure distribution for different surfaces: pyramid, hemisphere, cylinder, and grid-like morphology at an external loading pressure of 5 kPa.

confirmed to distinguish the pressure of ~1 Pa (Fig. S11) and shows great repeatability in several repeated signals. Besides, when applying force on the TPPCN pressure sensing unit, it offers a short response time of ~80 ms and recovery time of ~120 ms (Fig. 3f), which is fast enough for most of the practical applications. In particular, compared with TPPCN membrane with multi-level structure and grid-like morphology, blank sample shows a ~100% decline in the sensibility (~2.46 kPa^{-1}), as well as an increased response/recovery time, indicating an enhanced sensing properties and effective microstructure. Figure 3g shows a response of TPPCN membrane to the pulsed pressure of 250 Pa, 1.0 kPa, and 5.0 kPa with an increased frequency from 0.5 to 1.0 Hz, and the reversible and reproducible electronic signal reveal good stability. Also, the long-term stability is further be investigated in 1000 repetitive cycles of repeated loading/unloading process, as illustrated in Fig. 3h. The inset shows a magnified region of the electrical responses. The output signal is almost identical and identifiable in each cycle. Thus, we believe that the TPPCN membrane possesses a long service life and exhibits good stability for practical applications. Finally, Fig. 3i and Table. S1 show a comparison of the sensing properties with similar reported works. Compared with nanofibrous membrane-based pressure sensors, it is in a high level. At the same time, the preparation process is of great convenience, expansibility and universality, which is important for commercialization.

Mechanism discussion and model analysis

To understand the working mechanism of TPPCN membrane pressure sensor, we observe and simplify the gap variation between the spatial multi-level layers during the loading process, which is shown in Fig. 4a–c. Generally, it can be seen that the

contact areas among each layer of TPPCN membrane increases with the applied pressure on the surface, which will generate more charge transport channels and result in the decline of resistance. A basic sensing unit with two-layer structure is simplified to postulate an equivalent circuit model. Thus, the resistance can be calculated by the equation:

$$\frac{1}{R} = \frac{1}{R_L} + \frac{L}{R_L + nR_C} \quad (2)$$

where R_L, R_C, and n are the resistance of single lay of TPPCN, contact interface, and the number of contact junction. During the whole loading process, R_L remains unchanged, while R_C will decrease with increased pressure, accompanied by varied contact distance and the number of contact junction. In the initial stage, the decrease in the contact distance results in dramatic enhancement of contact junction due to the effective interlocking between surfaces of each layer, which further leads to the total resistance to decrease rapidly. Therefore, a high GF value can be obtained. Then, the variation of resistance decreases slowly with increasing pressure, as new contact junction was difficult to form. Finally, it becomes steady in the high-pressure region. At this stage, all layers of the TPPCN membrane are in contact with each other in a flattened form.

Moreover, as is widely accepted that a high and local stress concentration will be produced at the protrusions surrounding special surface[34,35]. It means an enhanced optimized efficiency of the contact area under the same applied force, which is beneficial to improve the sensibility and response/recovery time. To investigate the pressure distribution on the surface of TPPCN membrane, we simulate the pressure distribution on the grid-like morphology as well as another three microstructure that can be easily obtained by the template method, including pyramid, hemisphere, and cylinder (more simulation and modeling information are available in characterization section and Fig. S12). As shown in Fig. 4d–g, a loading of 5 kPa is applied and all these samples possess the stress concentration on their top protrusions area. Nevertheless, owing to sharper structure, more uneven stress distributions are observed from the samples of pyramid hemisphere, and cylinder structure. And samples of TPPCN membrane display more homogeneous pressure distribution along the altitude direction. Particularly, applied pressure can be transmitted to the root segment of adjacent peaks, indicating a small deformation in low pressure range. We believe that these architectural features endow them with different characteristics to meet the various requirements of the target application. Detailly, for our prepared sample, on the one hand, microgrid morphology enables TPPCN membrane to produce faster and larger deformation responses to pressure stimuli at smaller initial contact interfaces, resulting in a faster response time and 200% increase in initial GF value (compared with TPPCN-blank). Another key point to mention is the rough surface formed by the CCNTs loading, which is of great significance to the enhancement of detection limit and response time (Fig. S13). The CCNTs-modified surface enables the TPPCN membrane to produce stable signal response even under low stress. On the other hand, when the initial contact junctios at the top stress region achieve saturation in small deformation and loading force. The spatial multi-level interlocking structures provide more new contact junctions at high pressures. Similarly, enhanced contact areas caused by them can further compensate for the whole resistance variation. Therefore, the relative resistance variation still exhibits linearity within the large pressure range. To sum up, synergistic contribution of spatial multi-level structure and grid-like morphology enables a fast response/recover time, good sensibility, and wide-range detection linearity of TPPCN membrane.

Versatile applications of the TPPCN membrane

Owing to the good electromechanical performance of the prepared TPPCN membrane, it can be potentially used as wearable electronics. Here, we demonstrate how it can enable various proof-of-concept applications such as tactile strain sensor, temperature sensor, wearable heater, and triboelectric nanogenerator (TENG). Details of all devices preparation process and characterization are available in supporting information.

We first demonstrate its use as tactile sensor, results are shown in Fig. 5. TPPCN membranes used as sensing unit are assembled into a simple 'fabric piano', of which Cu wires and PDMS film are used as signal transmission lines and encapsulation enclosures (inset of Fig. 5a). As shown in Fig. 5a, the fabric piano possesses four signal channels, which can respond to four tactile signals independently at the same time. Before it, we demonstrated the positive relationship between the peak value and applied pressure. Similarly, the diversity of signal peaks is also of great importance for the application of sensors. For instance, a single signal pattern obviously cannot satisfy the vivid melody of piano. Hence, four different kinds of configuration of pressure signals including sine, Arb, half-sine, and square waveforms are vividly imitated with the same magnitude and frequency by controlling the time of pressure and the applied force. What's more, among these that have been displayed, signal with Arb and square form is selected to combine and simulate interesting Morse signal. As shown in Fig. 5b, well-organized lasting squeezing and rapid tapping could generate a series of signal peaks in a continuous manner that can be identified as points and lines of Morse code. Thus, information with actual meanings can be transformed. A demonstration of the letters including 'T', 'P', 'C', and 'N' is displayed as an example. Furthermore, to take advantage of good wearability and processibility, a conventional textile process is utilized to decorate TPPCN membrane to braided fabrics to form a monolithic sensing array (6 cm × 6 cm with 4 × 4 arrays, (Fig. 5c) for force mapping. With the assistance of more signal processors, these sensing fabrics could be used for gravity/pressure sensing in spatial area. As shown in Fig. 5c (II), four objects with weight of 2.5, 4, 7.5, and 45 g are placed at different locations, respectively. Evidently, the pressure distribution of them can be clearly identified with different color in the 3D Plot of R_0/R of the sensor array. Similarly, in another interesting example, five TPPCN membrane sensors are decorated on the glove. When holding the beaker with 100 mL and 200 mL water with glove, different pressure signals can be monitored, as shown in Fig. 5e. The resistance variation of each sensors is recorded and labeled in the schematic. Also, same experiments were operated using the glove with sensors attached to the arthrosis, a similar pressure distribution can be recorded and obtained when the volunteer hits an object (Fig. 5e). Apart from the pressure sensing applications, this obtained TPPCN membrane also shows an outstanding potential to be used for the detection of physiological signals and body motions. Here, we also do some simple trials, in which TPPCN is attached to a different area in the human body for detecting various motions. As illustrated in Fig. 5d, TPPCN membrane sensors displays a battery of sensitive signals corresponding to finger bending (Fig. 5d (I)), cheek blowing (Fig. 5d (II)), head nodding (Fig. 5d (III)), jumping (Fig. 5d (IV)), pulse vibrating (Fig. 5d (V)) and elbow bending (Fig. 5d (VI)). These signals contain large strains from body movement, moderate drafting from muscle expansion and contraction, and weak squeezing from pulse pulsations, which varies in intensity and frequency. Nevertheless, all of these show good repeatability, reliability, and reversibility, indicating the fine applicability and stability of prepared TPPCN membrane to the detection of human motion in a full range.

Human body temperature is of great importance to indicate various syndromes (e.g., influenza, metabolism disorders, and

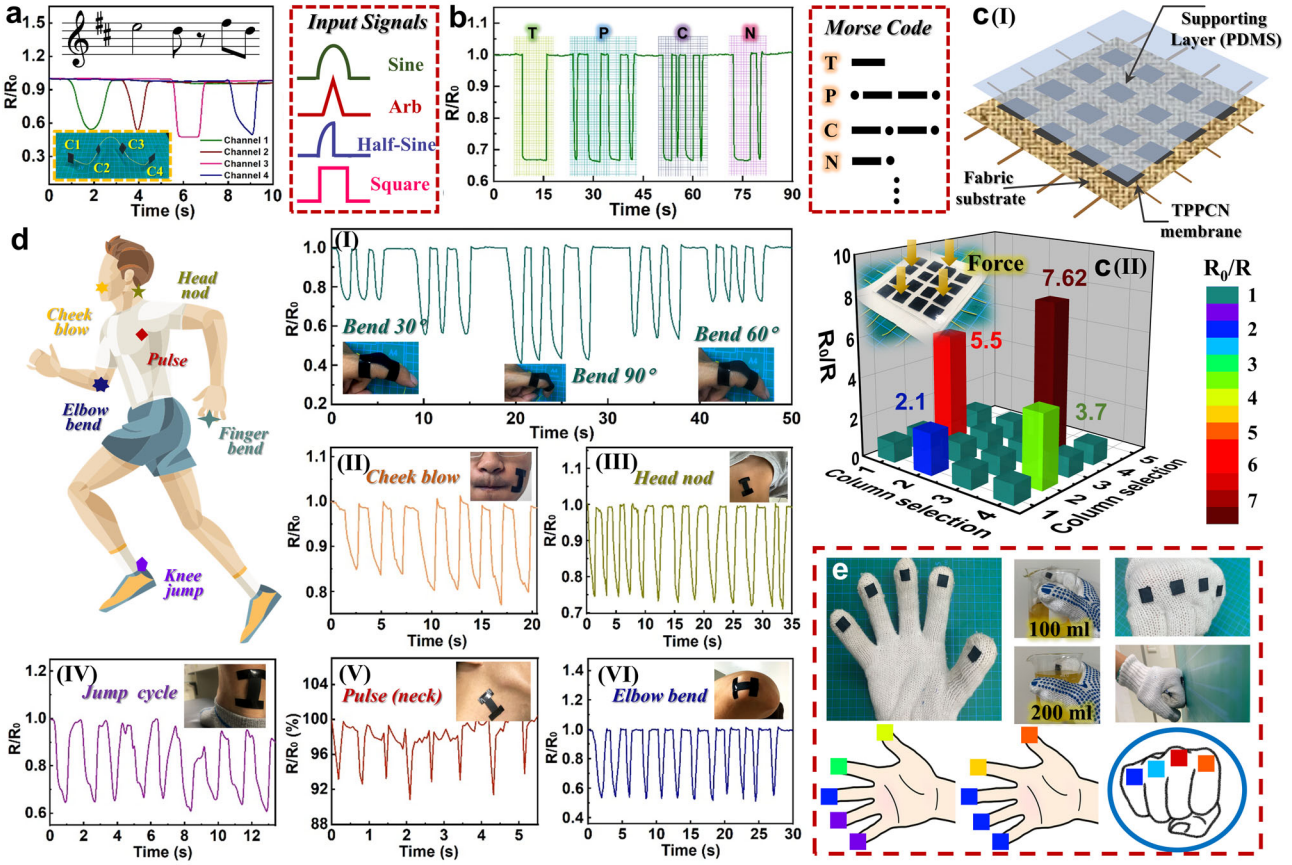

Fig. 5 Demonstrations of the TPPCN tactile sensor in various applications. a TPPCN membrane is fabricated as fabric piano to export four kinds of signal. **b** Morse code generation by signal with Arb and square form on the sensor surface. **c** Schematic diagram of the pressure sensor array (4 × 4 pixels) fabricated by TPPCN membranes and detection of applied pressure of the spatial pressure distribution. **d** Signals monitoring of whole-body using TPPCN membrane attached to different parts, which are marked by patterns in different colors in the human body model. **e** Photo of the several TPPCN membrane sensors attached to the figures and joint, photos of holding beakers with different volumes of water and hitting objects by hand, and the corresponding force distribution.

inflammation) and current state of the body. It is imperative to maintain a constant body temperature or to detect and alert for abnormal temperature variation. Owing to a great conductivity, TPPCN membrane can be used for electric-thermal conversion, results are shown in Fig. 6. The simultaneous temperature variation is shown in the time curves (Fig. 6b). As we can see, when the electric field is added to the TPPCN membrane, the temperature increases rapidly and reaches an equilibrium temperature subsequently. The heating temperature increases with applied voltage increased from 0.5 to 2.0 V. As long as 60 s is energized at a small voltage of 2 V, the temperature up to 70 °C can be achieved, indicating a high heating efficiency. Figure 6d shows the IR images of the heating process under a voltage of 5 V. Several typical dynamic temperatures of 35, 50, 75, and 100 °C during the heating process are recorded and displayed. Especially, this is an interesting current detection device. We use thermochromic PDMS to do an encapsulation to TPPCN membrane. When the current is turned on, Joule heat will cause obvious color change in PDMS (Fig. 6e), which plays an important warning role. Besides, cycle test of heating/cooling process is performed (Fig. 6c). A suitable circulation temperature of 33–50 °C (within the normal physiological signs) is selected. During each cycle, a voltage of 2 V is used to the TPPCN membrane until the resulting temperature reached ~50 °C. Then, the power supply was turned off until the sample temperature decreased to ~33 °C. The sample remains unaffected for several cycles, demonstrating the thermal stability and cyclability of the prepared TPPCN membrane. For the temperature sensing performance, the temperature and resistance variation of the sample are measured in real-time heating process simultaneously (Fig. 6f). TPPCN membrane shows an obvious thermosensitive property that the resistance decreases with increasing temperature. And the GF value is calculated to be 3.41 and 16.6% °C^{-1} among the temperature range of 20–85 °C and 85–100 °C, respectively. In another two experiments (Fig. 6g, h), significant response peaks can be observed when hot water and ice water are respectively close to TPPCN membrane with constant temperature (75 °C and 20 °C). To sum up, all these results indicate its potential applications in personal thermal management.

Harvesting energy from environments or human movement is both attractive and technically feasible for wearable electronics. And the cooperativity between soft materials and nanotechnology has yielded infusive advancements in nanogenerators. The assembled nanogenerator exhibits a typical sandwich structure, where CCNTs-doped PDMS and TPPCN membrane act as triboelectric layer and the electrode (Fig. 7a, digital image of prepared TENG are shown inset of Fig. 7e). Interface between CCNTs-doped-PDMS and TPPCN membrane is shown in Fig. S14. Figure 7b schematically exhibits the configuration and detailed working principle of the TENG. The equivalent charges with opposite polarities are formed between PDMS film and Al foil (Fig. 7b (I)). When the Al foil separates from the TPPCN, an electrical potential difference is formed between these two surfaces with oppositely charged owing to the difference in the ability to capture charge. Subsequently, transient electrons flow from the electrode to the ground to generate a current pulse until a new electrostatic

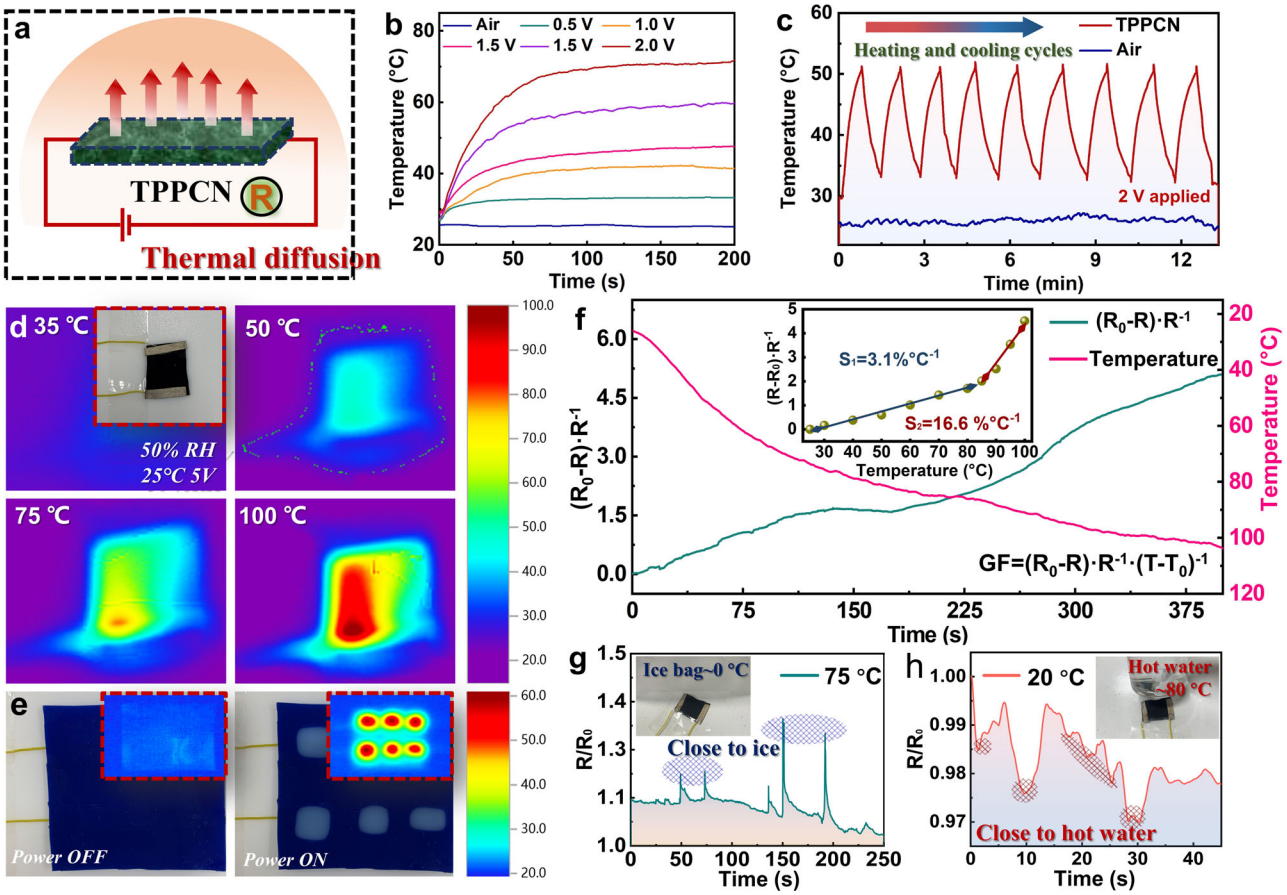

Fig. 6 Electric- thermal performance of TPPCN membrane. a Wearable TPPCN membrane as a thermal heater. **b** Temperature curves of the TPPCN membrane under the electric field of different voltage. **c** Repeatable behavior when heating the TPPCN membrane. **d** IR images of TPPCN membrane upon applying input voltages of about 5 V. **e** Demonstration of thermochromism of membrane materials used as a warning device. **f** Relative resistance change of obtained TPPCN membrane with the increased temperature. **g, h** Resistance responds upon the variation in temperature.

equilibrium is achieved. Thus, continuous contact/separation process will produce continuous alternative current. Output voltage is shown in Fig. 7c, d with an increased pressure and frequency. TENG with area of 40 × 40 mm could generate a typical voltage of 78 V. Also, corresponding current output is shown in Fig. 7e, and 0.45 μA is obtained. Furthermore, TENG is linked to LEDs in a rectified circuit (Fig. 7f) as a self-powered system. After repeat pressing process, LEDs are readily lighted, indicating a potential possibility for the applications in the field of indicator lights or energy collection equipment.

DISCUSSION

In summary, we developed a combined strategy of electrospinning and in situ polymerization to prepare CCNTs/PEDOT@PU/CCNTs (TPPCN) nanofibrous membrane with spatial multi-level structure and grid-like morphology. Experimental data and theoretical modeling analysis prove that the synergistic contribution of these special structure enables a fast response/recovery time (80 ms and 120 ms), good sensibility of 5.13 and 0.14 kPa^{-1} in the linear ranges of 0–1.0 and 1.0–8.0 kPa. As a result, it can be used to detect a variety of pressure stimuli including human movement, pulse, and gravity/pressure sensing in spatial areas. Additionally, as a platform to support integration and function expansion, we further demonstrate its potential applications for electric-thermal conversion and energy harvesting (TENG) devices. Totally, we believe that the results of the present work will provide some beneficial idea for the preparation of micro-structure nanofibrous membrane and inspires an opportunity for the function expansion of wearable electronic devices.

METHODS

Materials

Polyurethane (PU, Mw = 110, 000) was purchased from Sigma-Aldrich Chemical Co, USA. Carboxylated carbon nanotubes (CCNTs) was received from Nanjing XFNANO Materials Tech Co., Ltd, and their length and diameter are 5–10 μm and 10–30 nm, respectively. 3,4-Ethylenedioxythiophene (EDOT, 97%), N, N-Dimethylformamide (DMF, 99.5%), tetrahydrofuran (THF, 99.5%), ferric chloride ($FeCl_3$, 98%) and citric acid (CA, 98%), ethyl alcohol (EtOH, 99.5%) and cyclohexane (CYH, 99.5%) were provides by FUJIFILM Wako Pure Chemical Corporation, Japan. All chemicals were used as received without further purification.

Preparation of matrix membrane with hierarchical structure and grid-like morphology

PU/CCNTs nanofibrous membrane was prepared *via* conventional electrospinning technology using a metal mesh as receiving device. In a typical process, 1.6 g of PU granules and relative proportion of CCNTs were dissolved in 8.4 mL of DMF/THF (mass ratio of 1:1) mixture with mass ratio of 16 wt%. Especially, 0.32 g citric acid (CA) was added as complexing agent for the further ion adsorption and in situ polymerization. The resultant mixture was mechanically stirred for 12 h to obtain a homogeneous spinning solution at a temperature of 65 °C. Detailed electrospinning parameters include a voltage of 13.5 kV, the flow rate of 1.5 mL L^{-1}, and receiving distance of 15 cm. Afterwards, obtained samples were placed in an oven at 50 °C for 5 h to remove the residual solvent.

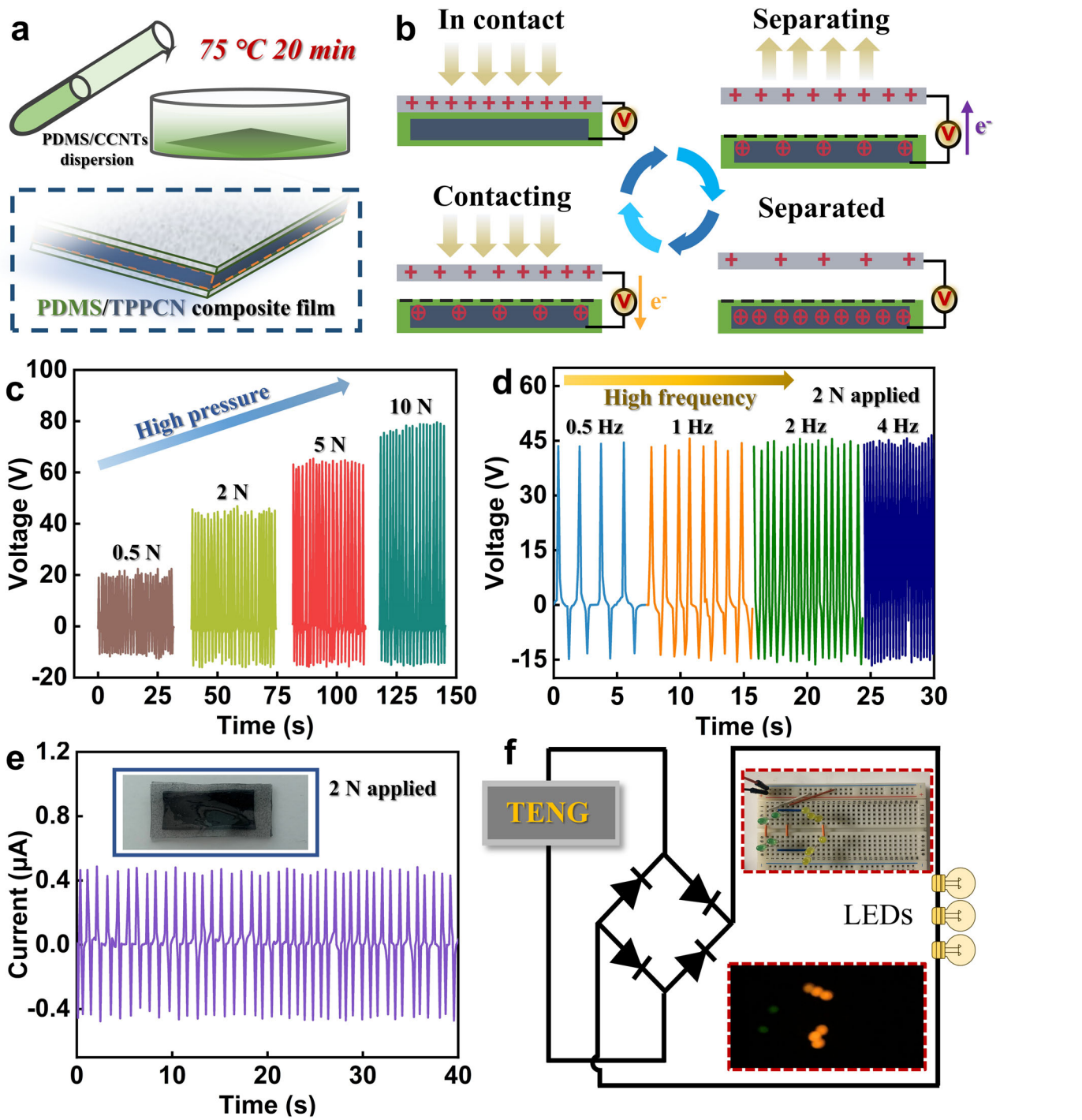

Fig. 7 Assembly and characterization of TPPCN-based TENG. a, b Preparation and works mechanism of TPPCN-based TENG with sandwich structure. **c–e** Output voltage of TENG with increased pressure, frequency, and corresponding output current with 2 N force applied. **f** LEDs in series were instantly turned on by a TENG.

Preparation of CCNTs/PEDOT@PCN nanofibrous membrane

PCN membrane was treated with plasma at a discharge power of 30 W for 150 s for necessary hydrophilic modification. Then, it was immersed in $FeCl_3$ solution (ethyl alcohol solvent, 0.01 M, 5 min) for an enough ion adsorption, followed by drying in an oven at 70 °C for 3 min. Obtained PCN-Fe^{3+} samples were soaked in EDOT monomer (cyclohexane solvent, 0.08 M) at room temperature for polyreaction. After washing several times with ethyl alcohol and drying in oven at 30 °C, PPCN membrane was obtained. Finally, PPCN membrane was immersed into the CCNTs dispersion (ethyl alcohol solvent, 1.5 mg L^{-1}) and then experienced ultrasonication for 45 min. After repeatedly rinsed with ethanol several times to detach the impurity and then dried in an oven at 60 °C for 5 h, the electrically conductive CCNTs @PPCN (named TPPCN) membrane was finally prepared. For comparison, the TPPCN membrane without special structure and morphology (TPPCN-blank) was fabricated. In detail, it was prepared by using traditional aluminum foil as the receiver. And following electrical activation process is the same as TPPCN film, including same PEDOT polymerization parameters and CNTs loading parameters.

DATA AVAILABILITY

The data that support the findings of this study are available from the corresponding authors upon reasonable request.

Received: 18 January 2022; Accepted: 17 May 2022;
Published online: 03 June 2022

REFERENCES

1. Xiong, J., Chen, J. & Lee, P. S. Functional fibers and fabrics for soft robotics, wearables, and human–robot interface. *Adv. Mater.* **33**, 2002640 (2021).
2. Rich, S. I., Wood, R. J. & Majidi, C. Untethered soft robotics. *Nat. Electron* **1**, 102–112 (2018).
3. Peng, B., Zhao, F., Ping, J. & Ying, Y. Recent advances in nanomaterial-enabled wearable sensors: material synthesis, sensor design, and personal health monitoring. *Small* **16**, 2002681 (2020).
4. Guo, H. et al. Artificially innervated self-healing foams as synthetic piezo-impedance sensor skins. *Nat. Commun.* **11**, 5747 (2020).
5. Iqbal, S. M. A., Mahgoub, I., Du, E., Leavitt, M. A. & Asghar, W. Advances in healthcare wearable devices. *npj Flex. Electron* **5**, 9 (2021).
6. Hong, S. Y. et al. Stretchable active matrix temperature sensor array of polyaniline nanofibers for electronic skin. *Adv. Mater.* **28**, 930–935 (2016).
7. Wang, P. et al. Surface engineering *via* self-assembly on PEDOT: PSS fibers: biomimetic fluff-like morphology and sensing application. *Chem. Eng. J.* **425**, 131551 (2021).
8. Chen, D. & Pei, Q. Electronic muscles and skins: a review of soft sensors and actuators. *Chem. Rev.* **117**, 11239–11268 (2017).
9. Kim, T. et al. Supersonically sprayed washable, wearable, stretchable, hydrophobic, and antibacterial rGO/AgNW fabric for multifunctional sensors and supercapacitors. *ACS Appl. Mater. Interfaces* **13**, 10013–10025 (2021).
10. Bai, J. et al. Facile preparation and high performance of wearable strain sensors based on ionically cross-linked composite hydrogels. *Sci. China Mater.* **64**, 942–952 (2021).
11. Zhang, C. et al. Highly adhesive and self-healing γ-PGA/ PEDOT: PSS conductive hydrogels enabled by multiple hydrogen bonding for wearable electronics. *Nano. Energy* **95**, 106991 (2022).
12. Xiong, Y. et al. A flexible, ultra-highly sensitive and stable capacitive pressure sensor with convex microarrays for motion and health monitoring. *Nano Energy* **70**, 104436 (2020).
13. Masihi, S. et al. Highly sensitive porous PDMS-based capacitive pressure sensors fabricated on fabric platform for wearable applications. *ACS Sens* **6**, 938–949 (2021).
14. Zhang, Y. et al. Ultra-stretchable monofilament flexible sensor with low hysteresis and linearity based on MWCNTs/Ecoflex composite materials. *Macromol. Mater. Eng*. 2100113 (2021).
15. Hwang, J., Kim, Y., Yang, H. & Oh, J. H. Fabrication of hierarchically porous structured PDMS composites and their application as a flexible capacitive pressure sensor. *Compos. B. Eng.* **211**, 108607 (2021).
16. Wang, L. et al. Highly stretchable, anti-corrosive and wearable strain sensors based on the PDMS/CNTs decorated elastomer nanofiber composite. *Chem. Eng. J.* **362**, 89–98 (2019).
17. Wang, Y., Yokota, T. & Someya, T. Electrospun nanofiber-based soft electronics. *NPG Asia Mater.* **13**, 22 (2021).
18. Sharma, S. et al. Hydrogen-bond-triggered hybrid nanofibrous membrane-based wearable pressure sensor with ultrahigh sensitivity over a broad pressure range. *ACS Nano* **15**, 4380–4393 (2021).
19. Yu, P. et al. All-fabric ultrathin capacitive sensor with high pressure sensitivity and broad detection range for electronic skin. *ACS Appl. Mater. Interfaces* **13**, 24062–24069 (2021).
20. Chinnappan, A., Baskar, C., Baskar, S., Ratheesh, G. & Ramakrishna, S. An overview of electrospun nanofibers and their application in energy storage, sensors and wearable/flexible electronics. *J. Mater. Chem. C.* **5**, 12657–12673 (2017).
21. Xue, J., Wu, T., Dai, Y. & Xia, Y. Electrospinning and electrospun nanofibers: methods, materials, and applications. *Chem. Rev.* **119**, 5298–5415 (2019).
22. Soares, R. M. D., Siqueira, N. M., Prabhakaram, M. P. & Ramakrishna, S. Electrospinning and electrospray of bio-based and natural polymers for biomaterials development. *Mater. Sci. Eng., C.* **92**, 969–982 (2018).
23. Zulqarnain, M. et al. A flexible ECG patch compatible with NFC RF communication. *npj Flex. Electron* **4**, 13 (2020).
24. Hwang, T.-Y. et al. A noble gas sensor platform: linear dense assemblies of single-walled carbon nanotubes (LACNTs) in a multi-layered ceramic/metal electrode system (MLES). *J. Mater. Chem. C.* **6**, 972–979 (2018).
25. Yang, J. C. et al. Microstructured porous pyramid-based ultrahigh sensitive pressure sensor insensitive to strain and temperature. *ACS Appl. Mater. Interfaces* **11**, 19472–19480 (2019).
26. Park, H. et al. Stretchable array of highly sensitive pressure sensors consisting of polyaniline nanofibers and Au-coated polydimethylsiloxane micropillars. *ACS Nano* **9**, 9974–9985 (2015).
27. Lee, K. Y. et al. Fully packaged self-powered triboelectric pressure sensor using hemispheres-array. *Adv. Energy Mater.* **6**, 1502566 (2016).
28. Yue, O. et al. Spider-web and ant-tentacle doubly bio-inspired multifunctional self-powered electronic skin with hierarchical nanostructure. *Adv. Sci.* 2004377 (2021).
29. Han, S. et al. High-performance pressure sensors based on 3D microstructure fabricated by a facile transfer technology. *Adv. Mater. Technol.* **4**, 1800640 (2019).
30. Wang, H. et al. Bioinspired fluffy fabric with in situ grown carbon nanotubes for ultrasensitive wearable airflow sensor. *Adv. Mater.* **32**, 1908214 (2020).
31. Pang, Y. et al. Epidermis microstructure inspired graphene pressure sensor with random distributed spinosum for high sensitivity and large linearity. *ACS Nano* **12**, 2346–2354 (2018).
32. Zhu, J., Yang, X., Zhou, Z., Ren, Y. & Xing, Y. Using folding structure to enhance measurement range, sensitivity of the flexible sensors: a simple, eco-friendly, and effective method. *Adv. Mater. Technol.* **6**, 2001216 (2021).
33. Wang, X., Liu, X. & Schubert, D. W. Highly sensitive ultrathin flexible thermoplastic Polyurethane/Carbon black fibrous film strain sensor with adjustable scaffold networks. *Nano-Micro Lett.* **13**, 64 (2021).
34. Qin, J. et al. Flexible and stretchable capacitive sensors with different microstructures. *Adv. Mater.* 2008267 (2021).
35. Ruth, S. R. A. & Bao, Z. Designing tunable capacitive pressure sensors based on material properties and microstructure geometry. *ACS Appl. Mater. Interfaces* **12**, 58301–58316 (2020).

ACKNOWLEDGEMENTS

This work was supported by JSPS KAKENHI (Grant numbers JP20H00288 and JP19K14032).

AUTHOR CONTRIBUTIONS

C.Z. and M.W. conceived and designed the work; H.M. supervised the research; L.D. fabricated the membrane-based TENG and characterized the date; J.W. analyzed the electric-thermal performance. M.W. wrote the manuscript; C.Z., J.S. and Q.G. revised the manuscript; All authors read and approved the final manuscript.

COMPETING INTERESTS

The authors declare no competing interests.

ADDITIONAL INFORMATION

Supplementary information The online version contains supplementary material available at https://doi.org/10.1038/s41528-022-00171-x.

Correspondence and requests for materials should be addressed to Chunhong Zhu or Hideaki Morikawa.

Reprints and permission information is available at http://www.nature.com/reprints

Publisher's note Springer Nature remains neutral with regard to jurisdictional claims in published maps and institutional affiliations.